

Lucía Romero, Esther Pueyo, Martin Fink and Blanca Rodríguez
Am J Physiol Heart Circ Physiol 297:1436-1445, 2009. First published Jul 31, 2009;
doi:10.1152/ajpheart.00263.2009

You might find this additional information useful...

This article cites 60 articles, 39 of which you can access free at:

<http://ajpheart.physiology.org/cgi/content/full/297/4/H1436#BIBL>

Updated information and services including high-resolution figures, can be found at:

<http://ajpheart.physiology.org/cgi/content/full/297/4/H1436>

Additional material and information about *AJP - Heart and Circulatory Physiology* can be found at:

<http://www.the-aps.org/publications/ajpheart>

This information is current as of October 23, 2009 .

Impact of ionic current variability on human ventricular cellular electrophysiology

Lucía Romero,^{1,2} Esther Pueyo,^{2,4} Martin Fink,³ and Blanca Rodríguez²

¹Instituto de Investigación Interuniversitario en Bioingeniería y Tecnología Orientada al Ser Humano, Universidad Politécnica de Valencia, Valencia, Spain; ²Oxford University Computing Laboratory, University of Oxford, Oxford, United Kingdom; ³Department of Physiology, Anatomy and Genetics, University of Oxford, Oxford, United Kingdom; and ⁴Instituto de Investigación en Ingeniería de Aragón, Universidad de Zaragoza, Zaragoza, Spain

Submitted 18 March 2009; accepted in final form 24 July 2009

Romero L, Pueyo E, Fink M, Rodríguez B. Impact of ionic current variability on human ventricular cellular electrophysiology. *Am J Physiol Heart Circ Physiol* 297: H1436–H1445, 2009. First published July 31, 2009; doi:10.1152/ajpheart.00263.2009.—Abnormalities in repolarization and its rate dependence are known to be related to increased proarrhythmic risk. A number of repolarization-related electrophysiological properties are commonly used as preclinical biomarkers of arrhythmic risk. However, the variability and complexity of repolarization mechanisms make the use of cellular biomarkers to predict arrhythmic risk preclinically challenging. Our goal is to investigate the role of ionic current properties and their variability in modulating cellular biomarkers of arrhythmic risk to improve risk stratification and identification in humans. A systematic investigation into the sensitivity of the main preclinical biomarkers of arrhythmic risk to changes in ionic current conductances and kinetics was performed using computer simulations. Four stimulation protocols were applied to the ten Tusscher and Panfilov human ventricular model to quantify the impact of ± 15 and $\pm 30\%$ variations in key model parameters on action potential (AP) properties, Ca^{2+} and Na^+ dynamics, and their rate dependence. Simulations show that, in humans, AP duration is moderately sensitive to changes in all repolarization current conductances and in L-type Ca^{2+} current (I_{CaL}) and slow component of the delayed rectifier current (I_{Ks}) inactivation kinetics. AP triangulation, however, is strongly dependent only on inward rectifier K^+ current (I_{K1}) and delayed rectifier current (I_{Kr}) conductances. Furthermore, AP rate dependence (i.e., AP duration rate adaptation and restitution properties) and intracellular Ca^{2+} and Na^+ levels are highly sensitive to both I_{CaL} and Na^+/K^+ pump current (I_{NaK}) properties. This study provides quantitative insights into the sensitivity of preclinical biomarkers of arrhythmic risk to variations in ionic current properties in humans. The results show the importance of sensitivity analysis as a powerful method for the in-depth validation of mathematical models in cardiac electrophysiology.

biological variability; arrhythmia; computer simulation

VENTRICULAR ARRHYTHMIAS can be caused by disease, genetic mutations, and drug cardiotoxicity, which lead to changes in ionic current properties and often result in repolarization abnormalities. Research into arrhythmia mechanisms has identified a number of cellular electrophysiological properties as potential biomarkers of arrhythmic risk (31), the majority of which are related to action potential (AP) shape and duration (APD) and, importantly, their rate dependence. The prediction of an increase in arrhythmic risk caused by ionic changes is

particularly important during the drug development process, as certain drugs can exhibit cardiotoxicity (i.e., unwanted side effects such as drug-induced alterations in cardiac ionic currents), which can put patients at risk of developing cardiac arrhythmias such as Torsades de Pointes (TdP). An optimal preclinical evaluation of drug cardiotoxicity is pivotal to reduce the huge costs of the drug development process since by the time a drug reaches the clinical trial stage, a large number of resources have been devoted to drug development. APD prolongation is considered the main preclinical biomarker of drug cardiotoxicity, because of its link to long QT syndrome. However, this has two important drawbacks: 1) the natural intra- and intersubject variability of APD, which makes it difficult to even define APD prolongation and 2) the variability in the proarrhythmic responses associated with ion current alterations that result in APD prolongation. In both cases variability arises not only through variability in one particular ion channel expression but also because of the complex electrophysiological interplay in which ion channel inhibition takes place. As recently described, this interplay varies due to both congenital and acquired mechanisms, including drug side effects as well as sex and age (44, 50, 51, 61).

The main goal of this study is to perform a systematic and quantitative investigation into how variability in ionic mechanisms modulates human ventricular cell electrophysiology and the main preclinical biomarkers of arrhythmic risk. The sensitivity of each biomarker to alterations in ionic currents properties was quantified using the most detailed human ventricular AP model to date, the ten Tusscher and Panfilov (2006) human ventricular AP model (TP06) (55), the predictive power of which has been demonstrated previously (37, 53). Validation of simulation results was performed by a comparison to experimental data obtained in human ventricular cardiomyocytes available in the literature. The findings of our study provide new insights into the ionic basis of the main preclinical biomarkers of arrhythmic risk. In addition, this study identifies new experimental data required for a further understanding of human cellular electrophysiology and demonstrates the importance of sensitivity analysis as a powerful method for systematic and in-depth validation of AP models in cardiac electrophysiology.

METHODS

Action Potential Model

The electrophysiological activity of a human ventricular epicardial cell was simulated using the TP06 model (55). Forward Euler integration with a time step of 0.02 ms was used to integrate the system of differential equations governing the cellular electrical behavior. To

Address for reprint requests and other correspondence: L. Romero, Inst. de Investigación Interuniversitario en Bioingeniería y Tecnología Orientada al Ser Humano (I3BH), Univ. Politécnica de Valencia, Camino de Vera s/n, 46022 Valencia, Spain (e-mail: lurope@eln.upv.es).

test the convergence, simulations with 0.001-ms time step displayed only minor differences (<5%) in the simulation results.

Stimulation Protocols

Four stimulation protocols were applied to the virtual human ventricular cardiomyocytes to characterize the main arrhythmic risk biomarkers proposed in the literature (see Fig. 1).

Steady-state AP and intracellular Ca^{2+} concentration properties. Steady-state AP and intracellular Ca^{2+} concentration ($[Ca^{2+}]_i$) transient properties such as APD, AP triangulation, and systolic and diastolic $[Ca^{2+}]_i$ levels have been proposed as arrhythmic risk biomarkers (2, 24, 40, 59). They were calculated from the simulations following the application of a train of 3,000 square transmembrane current pulses of 2-ms duration and twice the diastolic threshold at a cycle length (CL) of 1,000 ms. Stimulation currents were considered to

be K^+ currents as suggested in Hund et al. (27). Steady-state APD at 90 and 50% repolarization (APD_{90} and APD_{50} , respectively) and AP triangulation (defined as the difference between APD_{50} and APD_{90}) were calculated (Fig. 1A, top). Steady-state systolic and diastolic $[Ca^{2+}]_i$ at a CL of 1 (Fig. 1A, bottom) and 0.5 Hz were also determined.

APD restitution curves. Both theoretical and experimental studies have shown that steep restitution curves are related to an increased risk of occurrence of AP alternans and wavefront breakup, associated with the initiation and sustenance of lethal arrhythmias such as ventricular fibrillation (39, 60). APD_{90} restitution curves were constructed using both S1S2 and dynamic restitution protocols. The S1S2 restitution protocol consisted of a train of 10 square current pulses (S1) at a CL of 1,000 ms, followed by an extra stimulus (S2) applied at coupling intervals (CIs) ranging from 5,000 to 50 ms (CI step = 1 ms). The S1S2 restitution curve was obtained by plotting the APD_{90}

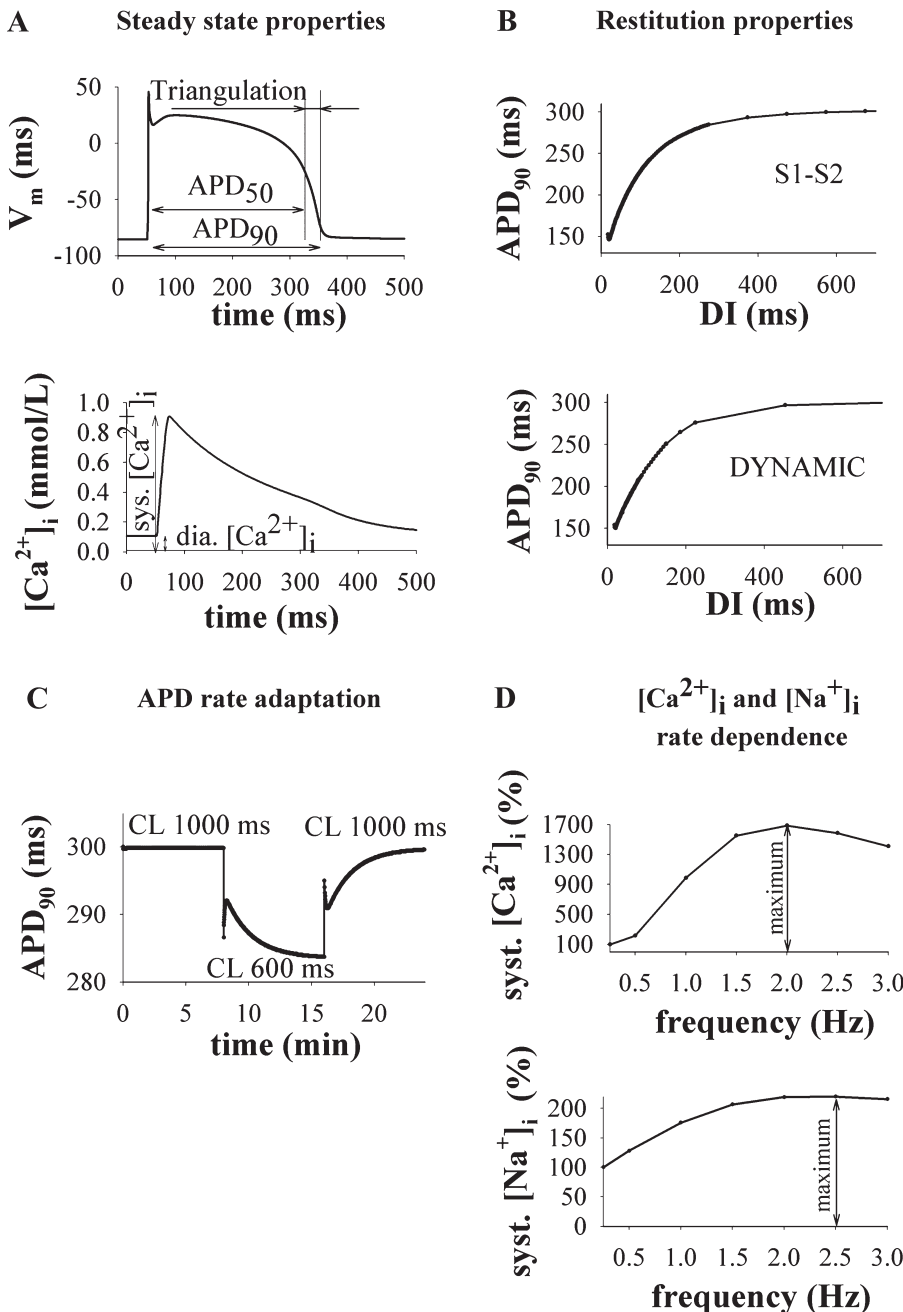


Fig. 1. Simulated electrophysiological activity of a human ventricular cardiomyocyte using the original ten Tusscher and Panfilov (2006) human ventricular action potential (AP) model (see Ref. 55). **A:** time course of the steady-state AP (top) and intracellular Ca^{2+} concentration ($[Ca^{2+}]_i$) transient (bottom) for 1-Hz stimulation frequency. APD_{50} and APD_{90} , AP duration (APD) at 50 and 90% repolarization, respectively. Triangulation is the difference between APD_{50} and APD_{90} . **B:** S1S2 (top) and dynamic (bottom) APD restitution curves. **C:** APD heart rate adaptation after step changes in cycle length (CL). **D:** normalized systolic (Syst) $[Ca^{2+}]_i$ (top) and intracellular Na^+ concentration ($[Na^+]_i$; bottom) relative to level at 0.25 Hz as a function of stimulation frequency. V_m , transmembrane potential; DI, diastolic (Dia) interval.

elicited by S2 versus the diastolic interval (DI) for each CI (Fig. 1B, top). The dynamic restitution curve [used to characterize drug reverse rate dependence (31)] was generated by plotting steady-state APD₉₀ versus steady-state DI for CLs ranging from 5,000 to 50 ms (Fig. 1B, bottom). The maximal slopes of S1S2 and dynamic restitution curves (slope_{max,S1S2} and slope_{max,Dyn}, respectively) were calculated.

APD rate adaptation to abrupt changes in CL. APD rate adaptation dynamics have been proposed as a clinical marker for arrhythmic risk (42). As in previous clinical and experimental studies (17, 30), APD₉₀ heart rate adaptation was characterized by recording APD₉₀ during the following stimulation protocol: first, pacing at CL of 1,000 ms for 8 min, then at CL of 600 ms for 8 min, and finally at CL of 1,000 ms for 8 min (Fig. 1C). APD₉₀ dynamics following each change in pacing rate were fitted to two exponential functions (41a), with time constants τ_{fast} and τ_{slow} , respectively. Because both time constants for both accelerating and decelerating rate transitions were similar, an APD₉₀ adaptation when CL changes from CL of 1,000 to 600 ms was applied.

Rate dependence of steady-state intracellular Na⁺ concentration and [Ca²⁺]_i. Because of the reported importance of intracellular Na⁺ concentration ([Na⁺]_i) and [Ca²⁺]_i dynamics in arrhythmogenesis (32, 36), changes in [Na⁺]_i and [Ca²⁺]_i levels with varying stimulation rates were investigated using a frequency staircase protocol. Cardiomyocytes were paced at increasingly fast frequencies (0.25, 0.5, 1, 1.5, 2, 2.5, and 3 Hz) for 10 min, and systolic [Ca²⁺]_i and [Na⁺]_i levels were recorded for each frequency and normalized to the respective levels at 0.25 Hz (Fig. 1D).

Sensitivity Analysis

A sensitivity analysis was performed in the model to investigate how natural variability or drug-induced alterations in ionic current properties might modulate preclinical biomarkers of arrhythmic risk. The ionic current properties considered in the sensitivity study were the maximal conductances and time constants of the main transmembrane ionic currents involved in AP repolarization, namely, maximal conductance (G_{CaL}) of the L-type Ca²⁺ current (I_{CaL}); activation gate time constant (τ_d), as well as its fast and slow voltage-dependent inactivation gate time constants (τ_{f2} and τ_f , respectively); maximal conductance (G_{Kr}) and activation and inactivation gate time constant (τ_{Xr1} and τ_{Xr2} , respectively) of the rapid component of the delayed rectifier current (I_{Kr}); maximal current conductance (G_{Ks}); and activation time constant (τ_{Xs}) of the slow component of the delayed rectifier current (I_{Ks}) and maximal conductance (G_{K1}) of the inward rectifier K⁺ current (I_{K1}), maximal activity of the Na⁺/K⁺ pump (G_{NaK}), and maximal activity of the Na⁺/Ca²⁺ exchanger (G_{NaCa}).

The sensitivity analysis was performed by varying one parameter at a time, by -30% and -15%, +15% and +30%, respectively. The magnitude of the changes imposed is in line with the natural variability reported experimentally in human ventricular tissue (15, 18, 28, 34, 52, 57, 58). Simulations using the four protocols described in *Simulation Protocols* were conducted for each parameter data set, and the results were compared with experimental data in the literature. A total of 5,220 simulations were run.

Data Analysis

For each electrophysiological characteristic “c” and parameter “p,” the indexes percentage of change ($D_{c,p,a}$) and sensitivities ($S_{c,p}$) were calculated as follows:

$$D_{c,p,a} = \frac{(C_{p,a} - C_{control})}{C_{control}} \cdot 100 \quad (1)$$

$$S_{c,p} = \frac{\Delta D_{c,p,a}}{\Delta a} = \frac{D_{c,p,+30\%} - D_{c,p,-30\%}}{0.6} \quad (2)$$

with $c_{p,a}$ and $c_{control}$ being the magnitude of the characteristic “c” when the parameter “p” is increased by “a” and under control conditions, respectively.

Moreover, to identify the model parameters that had a stronger influence on each electrophysiological characteristic, a relative sensitivity $r_{c,p}$ was calculated as the ratio between each $S_{c,p}$ and the maximum absolute value of $S_{c,p}$ obtained for that particular “c.”

RESULTS

Figures 2–7 illustrate the simulations results obtained using the protocols described in *METHODS*. Figure 2 depicts the time course of the simulated APs under control conditions and for 30% reduction of each parameter value. Figure 3 shows the relative sensitivities $r_{c,p}$ of all combinations of electrophysiological characteristics to parameter variations using a gray level scale. The effects of τ_d , τ_{Xr1} , τ_{f2} , and τ_{Xr2} changes on electrophysiological characteristics were negligible and thus are not shown. White indicates the strongest relative sensitivity among all parameters, whereas black means that the parameter and characteristic are completely independent. For each row, the maximum absolute sensitivity $S_{c,p}$ exerted in a particular characteristic “c” among all parameters is also shown as a percent value. Figures 4–6 show changes in steady-state AP, [Ca²⁺]_i dynamics, and rate adaptation of AP and [Ca²⁺]_i, respectively, caused by ± 15 and $\pm 30\%$ variations in model parameters. In each panel, experimentally recorded values of each electrophysiological property are represented as dotted horizontal lines, when available. In the following sections, the results obtained in the simulations are further described and discussed.

Steady-State AP Properties

Action potential duration. Simulations show that APD₉₀ is particularly sensitive to the inactivation kinetics properties of I_{Ks} and I_{CaL} (especially, τ_{Xs} and τ_f) and the maximum conductances of all currents involved in repolarization and, in particular, G_{CaL} , G_{Ks} , and G_{Kr} (Fig. 2, and 1st row of Fig. 3).

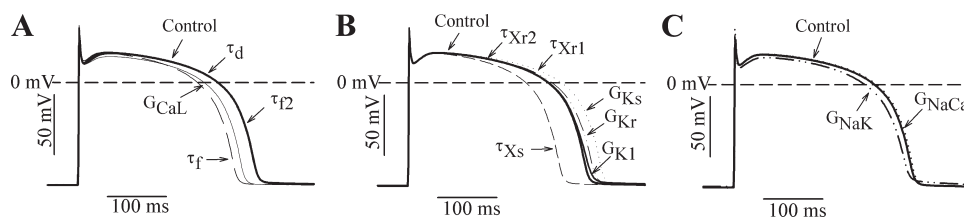


Fig. 2. Time course of the simulated AP under control conditions (thick solid line) and for 30% reduction in G_{CaL} (thin solid line), τ_d (thin short-dashed line), τ_f (thin long-dashed line), and τ_{f2} (thin dashed-dotted line) (A); G_{Ks} (thin short-dashed line), G_{Kr} (thin dashed-dotted line), G_{K1} (thick solid line), τ_{Xs} (thin dotted line), τ_{Xr1} (thick short-dashed line), and τ_{Xr2} (thick dashed plotted line) (B); and G_{NaK} (thick dashed-dotted line) and G_{NaCa} (thick dotted line) (C). See *METHODS* for definitions of abbreviations for conductances and time constants.

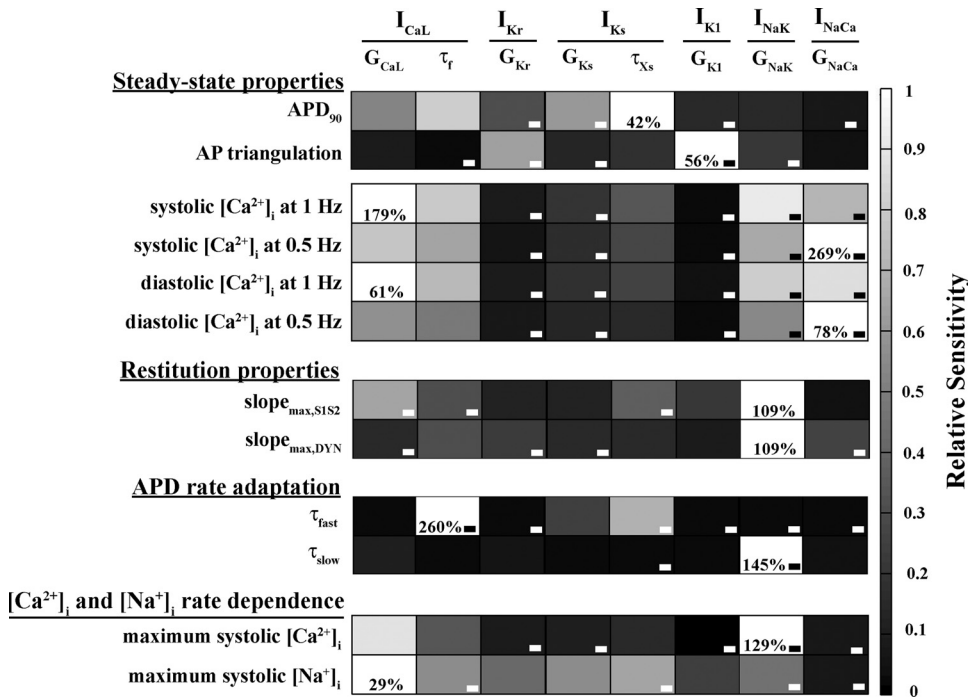


Fig. 3. Relative sensitivities of the electrophysiological properties (1st column) to changes in ionic current properties (1st row). A gray color scale is used. White indicates maximum relative sensitivity of a particular electrophysiological property among all parameters, whereas black indicates property and parameter are independent. Percentages in each white box indicate the maximum absolute sensitivity of the property correspondent to that row for all parameters. Negative sign indicates that property and parameter vary inversely. See METHODS for definitions of abbreviations for currents, slopes, conductance, and time constants.

Interestingly, as shown in Fig. 4A, 30% variations in the model parameters still result in simulated APD values within the physiological range of APD reported experimentally (12, 33), namely from 271 ± 13 to 351 ± 14 ms (dotted lines in Fig. 4A). Furthermore, consistent with experiments in human myocytes, the simulations show that a decrease in G_{CaL} results in APD₉₀ shortening (11, 34), whereas a decrease in G_{Kr} and G_{Ks} results in APD₉₀ prolongation (5, 21, 24, 29, 31). Interestingly, Na^+/K^+ pump current (I_{NaK}) block moderately reduces APD₉₀, in agreement with the effect of strophanthidin on the APD shown in experimental recordings on guinea pig cardiac myocytes (32). The results from Levi et al. (32) show that a

strophanthidin application results in an initial brief lengthening of APD because of a reduced outward current, followed by a sustained APD shortening caused by $[Na^+]_i$ accumulation and the subsequent increase in the reverse mode of the Na^+/Ca^{2+} exchange current (I_{NaCa}), which contributes to cell repolarization (14). These effects are reproduced in our simulations.

Action potential triangulation. Figure 3, second row, and Fig. 4B reveal the importance of G_{K1} and G_{Kr} in AP triangulation. This is consistent with the experimental data showing that I_{K1} block with barium leads to a 25% increase in AP triangulation in dog (4) and that I_{Kr} inhibition enhances AP triangulation in healthy (29) and diseased human myocytes

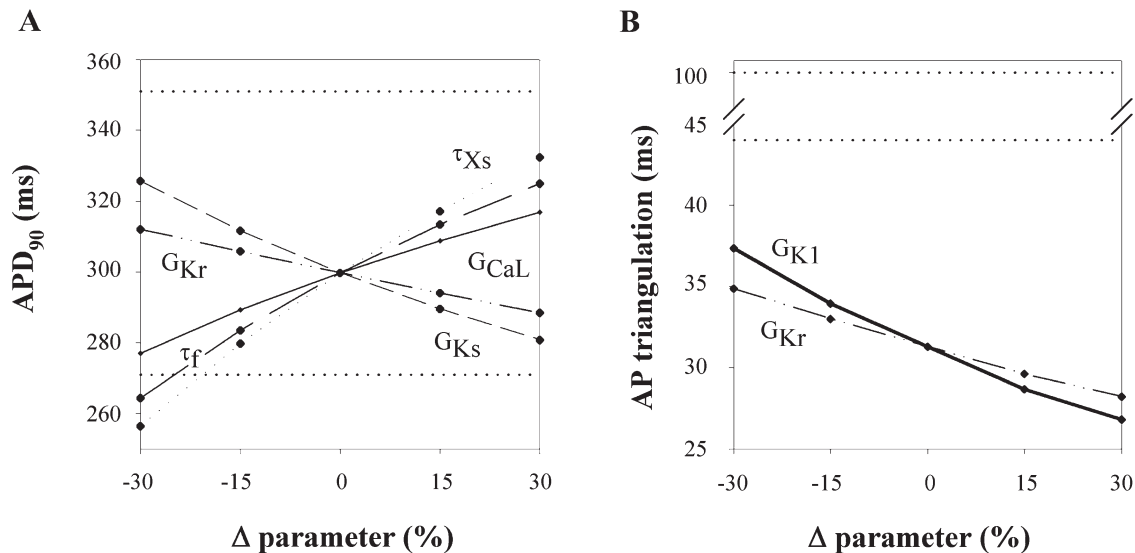


Fig. 4. Changes in steady-state APD (A) and AP triangulation (B) caused by variations on G_{Kr} , G_{CaL} , and G_{Ks} and in I_{CaL} inactivation and I_{Ks} activation gate time constants (τ_f and τ_{Xs} , respectively) and G_{Kr} and G_{K1} , respectively. The x-axis indicates percentage of parameter variation (Δ parameter). Horizontal dotted lines indicate experimental values reported in the literature (see Refs. 12, 33, 34).

(47), as well as in dog (31) and rabbit ventricular cells (24). However, simulated AP triangulation is 31 ms in control, whereas experimentally reported values are larger and vary in the range between 44 (33) and 100 ms (34) (Fig. 4B).

AP triangulation reflects relative changes between APD_{90} and APD_{50} , and it is roughly one order of magnitude smaller than APD_{90} (under control conditions, they are 31 and 299.8 ms, respectively). Thus a particular intervention can result in significant percent changes in AP triangulation in the presence of only slight changes in APD_{90} . Indeed, I_{K1} inhibition by 30% results in APD_{90} prolongation by 1.9%, no change in APD_{50} , and thus in a 16.1% increase in AP triangulation. In the case of G_{Kr} reduction, both APD_{90} and APD_{50} are prolonged (Fig. 2B), although APD_{50} to a smaller extent than APD_{90} , thus resulting in an increase of AP triangulation. By contrast, I_{Ks} modulation of APD_{90} and APD_{50} are similar and, therefore, AP triangulation remains unchanged.

Steady-State $[Ca^{2+}]_i$ Dynamics

The simulation results show that G_{CaL} and G_{NaCa} are key in determining both systolic and diastolic $[Ca^{2+}]_i$ levels, with G_{CaL} exerting the strongest influence at 1 Hz (179% sensitivity) and G_{NaCa} at 0.5 Hz (269% sensitivity) (see Fig. 3, rows 3–6, and Fig. 5). In addition, the I_{CaL} inactivation gate time

constant (τ_f) and G_{NaK} are also important determinants of $[Ca^{2+}]_i$ levels. These results are in agreement with experimental observations in human ventricular tissue (8, 22, 23, 48). However, as illustrated in Fig. 5, simulated $[Ca^{2+}]_i$ levels for control are smaller than the ones found in the literature (dotted lines), particularly for 0.5 Hz (3, 46).

Rate Adaptation

APD and $[Ca^{2+}]_i$ dependence with varying stimulation rates are known to be related to arrhythmogenesis, and here we investigate how ionic current properties modulate human rate dependence in ventricular cells.

SIS2 restitution curve. Figure 3, seventh row, highlights the importance of G_{NaK} , G_{CaL} , and to a lesser extent of I_{Ks} activation kinetics and I_{CaL} inactivation kinetics (τ_{Xs} and τ_f) in modulating $slope_{max,SIS2}$. $slope_{max,SIS2}$ is flattened by I_{NaK} inhibition but becomes steeper with the reduction in the remaining parameters (Fig. 6A). Figure 7, A and B, depicts the simulated restitution curves for the control and also for the 30% reduction in G_{NaK} , G_{CaL} , τ_{Xs} , and τ_f for DIs < 600 and 160 ms, respectively. Changes in restitution slope induced by parameter variations are dependent on DI. I_{CaL} inhibition increases the SIS2 restitution curve slope at DIs < 40 ms (and thus $slope_{max,SIS2}$) but flattens the curve at longer DIs (Fig.

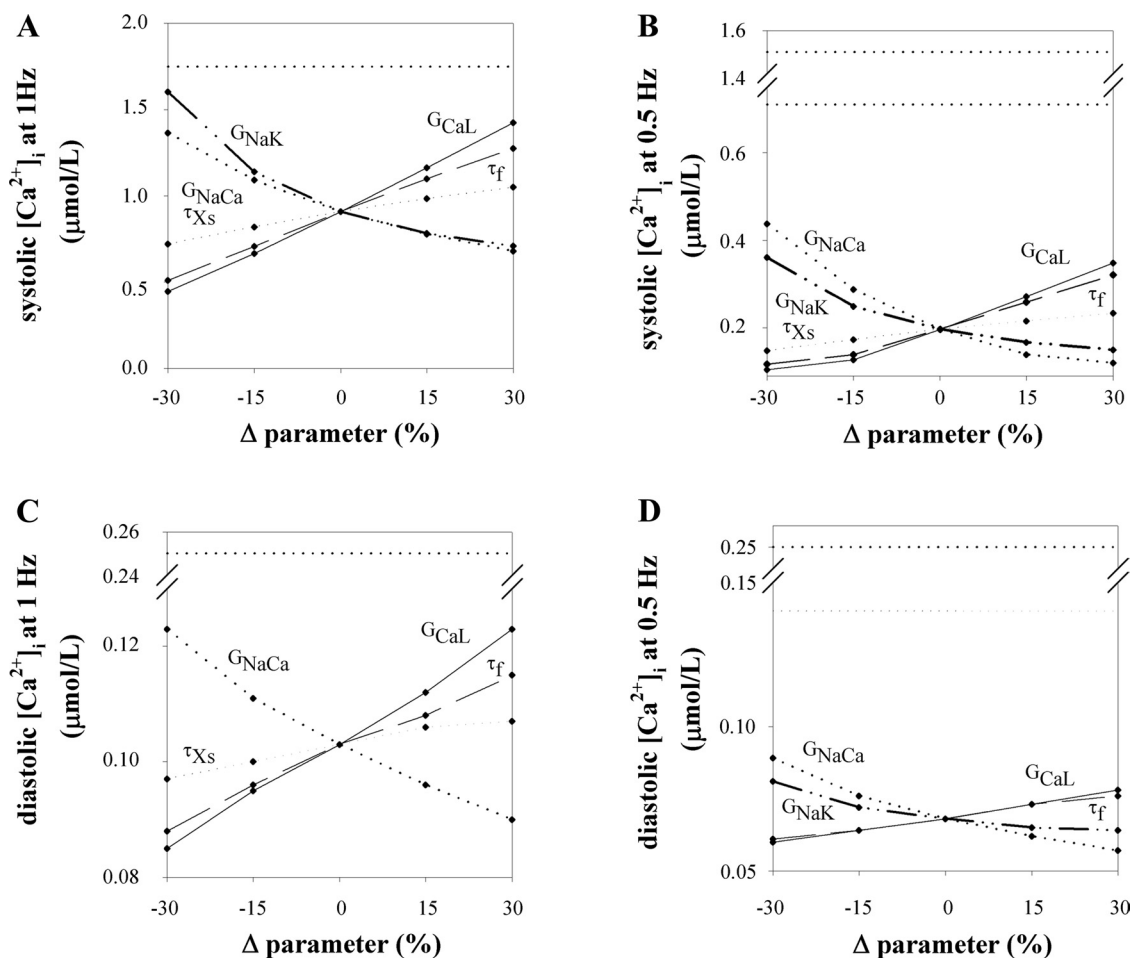


Fig. 5. Changes in steady-state systolic and diastolic $[Ca^{2+}]_i$ values at 1 (A and C) and 0.5 Hz (B and D) caused by variations on G_{CaL} , G_{NaK} , and G_{NaCa} and in I_{CaL} inactivation and I_{Ks} inactivation gate time constants (τ_f and τ_{Xs} , respectively). The x-axis indicates percentage of parameter variation (Δ parameter). Horizontal dotted lines depict experimental values reported in the literature (see Refs. 3, 46).

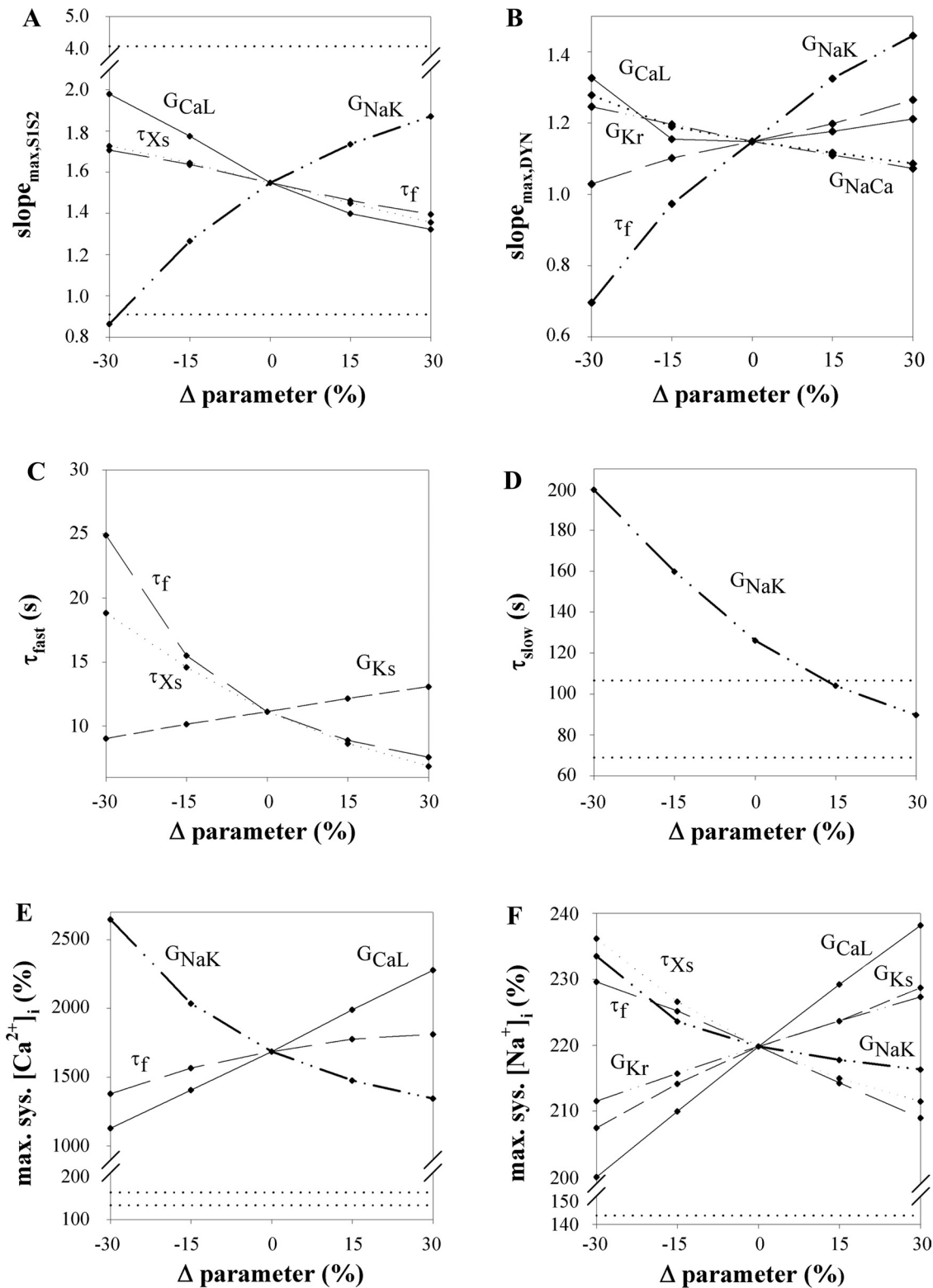


Fig. 6. Changes in restitution curves slopes: $\text{slope}_{\text{max,S1S2}}$ (A), $\text{slope}_{\text{max,Dyn}}$ (B), APD rate adaptation [τ_{fast} (C) and τ_{slow} (D)], and maximum systolic (Max Sys) $[\text{Ca}^{2+}]_i$ and $[\text{Na}^+]_i$ (E and F, respectively) with changes in G_{CaL} , G_{NaK} , G_{Kr} , and G_{NaCa} and in I_{CaL} and I_{Ks} gate time constant (τ_{f} and τ_{Xs} , respectively) as labeled next to each curve. The x-axis indicates percentage of parameter variation (Δ parameter). Horizontal dotted lines depict experimental values reported in the literature (see Refs. 17, 38, 40, 41).

7B), as shown experimentally using nisoldipine, an I_{CaL} blocker, on isolated rabbit ventricular myocytes (56). Similarly, faster I_{CaL} inactivation and I_{Ks} activation (i.e., decrease in τ_{f} and τ_{Xs}) flatten the S1S2 restitution curve at all DIs,

except for very short DIs (Fig. 7B). Importantly, 30% variations in all parameters result in $\text{slope}_{\text{max,S1S2}}$ still within the physiological range reported experimentally by Nash and co-workers (38), as shown in Fig. 6A.

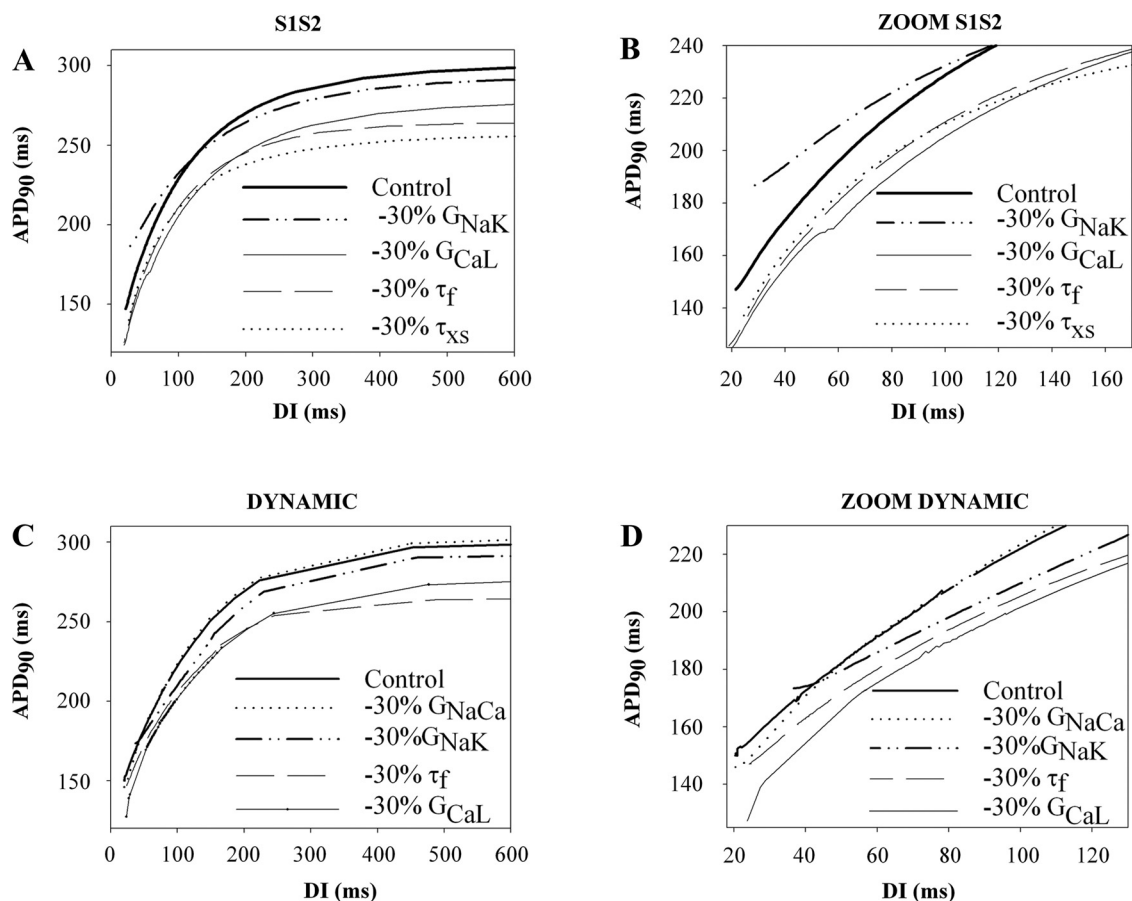


Fig. 7. S1S2 (A and B) and dynamic restitution curves (C and D) for control and for 30% reduction of model parameters for DI < 600 ms and DI < 160 ms, respectively.

Dynamic restitution curve. As for $\text{slope}_{\text{max,S1S2}}$, simulated $\text{slope}_{\text{max,Dyn}}$ depends strongly on G_{NaK} and, to a smaller extent, on G_{CaL} , G_{Kr} , and τ_f (Fig. 3, 8th row, and Fig. 6B). Our simulation results reveal that G_{CaL} reduction from +30 to -15% of the control value results in a slight flattening of the restitution curve (Fig. 6B), whereas for 30% G_{CaL} inhibition, the restitution curve flattens for DI > 60 ms and becomes steeper than in the control for DI < 60 ms (Fig. 7D). The experimental results in human myocytes show that I_{CaL} suppression in human myocytes significantly attenuates the rate-dependent abbreviation of APD for DI > 300 ms (34), which is in agreement with our simulations results. However, experimental (43) and theoretical (16, 19) studies in dog and guinea pig show that I_{CaL} inhibition results in a flattening of the restitution curve also at short DIs. This discrepancy with our simulation results in humans could be due to true animal species differences, heterogeneity in restitution properties (38), or the fact that the dependency of dynamic restitution curve slope on I_{CaL} properties is not well represented in the mathematical models.

Our simulation results also show that I_{Kr} block increases the dynamic restitution slope, as experimentally recorded in human myocytes (29). However, the experimental recordings by Jost et al. (29), as well as previous experimental and simulation studies in dog and guinea pig (25, 26), might suggest a more important contribution of I_{Kr} to rate-related alterations of repolarization than the one observed in our simulations. This could be due to animal species differences (7) and also to model deficiencies in the representation of repolarization mechanisms.

APD adaptation to sudden sustained changes in stimulation rate. As in experimental and clinical studies (17, 30), simulated APD rate adaptation follows two phases (rapid and slow) with time constants for control being $\tau_{\text{fast}} = 11$ ms and $\tau_{\text{slow}} = 121$ s, respectively, which are close to the experimental values reported by Franz and collaborators (dotted lines in Fig. 6) (17).

As shown in Fig. 3, eighth row, and in Fig. 6C, τ_{fast} is strongly dependent on I_{CaL} inactivation dynamics (τ_f), consistent with experiments in human ventricular myocytes (34), and also to a lesser extent on I_{Ks} properties (both τ_{xs} and G_{Ks}). In contrast, τ_{slow} is only significantly influenced by G_{NaK} (Fig. 3, 9th row), with Na^+/K^+ pump inhibition resulting in a prolonged τ_{slow} (Fig. 6D), consistent with experimental results in dog (6).

Rate dependence of ionic concentrations. As reported in experimental studies in human and other animal species (1, 23, 40, 41), simulated systolic $[\text{Ca}^{2+}]_i$ and $[\text{Na}^{2+}]_i$ levels increase with an increase in frequency, reaching a maximum at 2 and 2.5 Hz, respectively, for control model parameters (Fig. 1D). However, the effect of the increasing stimulation frequency on systolic $[\text{Ca}^{2+}]_i$ is significantly larger in the simulations than the one reported experimentally (40, 41) (Fig. 6, E and F, dotted lines).

Figure 3, 10th row, shows that the maximum systolic $[\text{Ca}^{2+}]_i$ is highly sensitive to G_{NaK} (with sensitivity = 114%) and also, although to a lesser extent, to G_{CaL} and τ_f . $[\text{Na}^+]_i$ frequency modulation, and thus the maximum systolic $[\text{Na}^+]_i$, is less sensitive to model parameters than maximum systolic

$[Ca^{2+}]_i$, with G_{CaL} being the parameter exerting the maximum influence maximum systolic $[Na^+]_i$ (sensitivity = 29%) followed by τ_{xs} , G_{Ks} , τ_f , G_{NaK} , and G_{Kr} (Fig. 3, last row, and Fig. 6F). The experimental results on the changes in $[Na^+]_i$ with varying pacing rate are scarce. Prieske et al. (41) reported an increase in $[Na^+]_i$ with an increasing pacing rate, consistent with our simulation results (see Fig. 1D, bottom). However, the maximum increment they observed was 44%, which is significantly smaller than the one observed in our simulations (120%). In addition, they measured a concentration of 15.9 mmol/l at 0.25 Hz, larger than the simulated value of 5.6 mmol/l for control.

DISCUSSION

The TP06 Human Ventricular Model

In this article, the most detailed human ventricular model to date, the TP06 model, was used to systematically investigate the ionic basis of electrophysiological properties related to arrhythmic risk in human ventricular cardiomyocytes. As described in the original articles (54, 55), three main types of data were used in the model development, namely, data on ionic currents, conductances, and kinetics; on steady-state AP and intracellular concentrations dynamics; and on frequency modulation of AP and intracellular concentrations. Many of the data were based on recordings in human ventricular tissue, but because of the scarcity of data from humans, the model parameter fitting was sometimes based on experimental data obtained from human atrium, cultured cells, and other animal species such as dog and guinea pig.

This study presents an analysis of the sensitivity of the model and, in particular, of the preclinical biomarkers of arrhythmic risk to changes in conductances and kinetics of the main ionic currents involved in repolarization. The applied changes in model parameters could represent natural intrasubject variability [as reported by Verkerk et al. (57), for instance] and/or the effects of specific pharmacological interventions or channel mutations on electrophysiological properties. The simulation results were compared with the experimental data recorded in human tissue, when available, under control conditions and following pharmacological interventions mimicking the parameter changes introduced in our analysis. The results show that steady-state APD and APD restitution curve properties as well as APD adaptation dynamics are well reproduced by the model, both in terms of their control conditions and how they are modulated by varying ionic current properties. Other properties such as AP triangulation and $[Ca^{2+}]_i$ and $[Na^+]_i$ levels show good qualitative agreement with the experimental results, but significant differences are observed quantitatively. Discrepancies between the experimental and simulated electrophysiological characteristics may lie on a parameter fitting not exclusively based on experimental human ventricular data because of the scarcity of data that characterize human ventricular electrophysiology. Thus the obtention of new experimental data will be very valuable for model improvement. This study demonstrates that sensitivity analysis, as performed in this study on the TP06 model, provides a good basis for the systematic validation and further improvement of AP models.

Sensitivity and Selectivity of Electrophysiological Biomarkers of Arrhythmic Risk

APD is the main preclinical biomarker used to assess the risk of TdP caused by drug-induced side effects or mutations. Our simulations show that APD is moderately sensitive (maximum sensitivity = 42%) to changes in maximal conductances of all currents involved in repolarization and also I_{Ks} and I_{CaL} kinetics (Fig. 3, 1st row). Thus the same APD value can be obtained for a variety of combinations of ionic current property values, without it providing any indication of arrhythmic risk stratification. The use of additional biomarkers is therefore needed to assess proarrhythmic risk preclinically based on cardiac cell electrophysiology.

The present study highlights important differences in the maximal sensitivity of electrophysiological properties associated with arrhythmic risk to changes in ionic current properties. The new insights provided could be key in improving the preclinical assessment of arrhythmic risk and also in identifying the potential mechanisms of arrhythmogenesis associated to particular subjects or interventions. For instance, the results of our study show that AP triangulation is mostly dependent on G_{K1} and, to a lesser extent, on G_{Kr} , as experimentally observed (4, 24, 29, 31). Thus increasing G_{K1} and G_{Kr} reduces AP triangulation, thus predicting a decrease in the risk of TdP occurrence. Moreover, as shown in Fig. 3, the steady-state $[Ca^{2+}]_i$ levels are highly dependent on both the conductance and kinetics of I_{CaL} but also on G_{NaK} and G_{NaCa} . Additional biomarkers such as APD rate adaptation dynamics and restitution properties as well as $[Ca^{2+}]_i$ and $[Na^+]_i$ levels are also highly sensitive to I_{CaL} and I_{NaK} properties. This highlights the importance of the two currents in cell homeostasis and arrhythmia mechanisms related to early afterdepolarizations and alternans.

Our results also show that the APD restitution curves become steeper for the enhanced activity of the Na^+/K^+ pump, as well as for slow I_{CaL} inactivation kinetics and I_{Ks} activation kinetics (i.e., large τ_f and τ_{xs} values), and thus the proarrhythmic potential of those interventions could be associated with an increased risk of alternans development, which is considered potentially proarrhythmic. However, other parameters, such as G_{CaL} , increase the slope of the restitution curves at small CIs while flattening the curve at higher CIs.

The results of the present study also highlight the need for new experimental data to further our understanding of the ionic basis of ventricular electrophysiology in humans. An experimental validation is required for the pivotal role of the Na^+/K^+ pump and the Na^+/Ca^{2+} exchanger in the restitution properties and frequency modulation of $[Ca^{2+}]_i$ levels suggested by the simulations. The significant effect of G_{CaL} and τ_f on steady-state $[Ca^{2+}]_i$, frequency modulation of $[Ca^{2+}]_i$ and $[Na^+]_i$, and restitution properties suggested by the simulations also needs experimental characterization. Furthermore, the experimental data confirming the role of I_{Ks} properties (and, in particular, τ_{xs} and G_{Ks}) in determining the slope of the S1S2 restitution curve, Ca^{2+} dynamics, APD, and maximum systolic $[Na^+]_i$ would be required to provide further insight into the role of I_{Ks} in human ventricular cell electrophysiology.

Limitations of the Study

In this study, a systematic analysis on the role of ionic current properties in modulating preclinical arrhythmic risk biomarkers has been performed using the most detailed human

ventricular model to date. Simulations using the model yield electrophysiological properties that are, in most cases, in good agreement with experimental data obtained using human ventricular myocytes. However, some quantitative differences are observed, often related to $[Ca^{2+}]_i$ levels, highlighting the need for further improvements in the model development, which would also benefit from additional experimental data. Because of the scarcity of experimental results in undiseased human myocytes, data from diseased human tissue and other animal species were also used to develop the original TP06 model and to evaluate the simulation results in this study. Thus discrepancies between simulation and experimental results might be due to true animal species differences or to the fact that the model is, in some aspects, not optimally configured to represent undiseased human ventricular electrophysiological behavior.

In addition, our simulations do not account for transient changes in K^+ concentration of the clefts surrounding the cells following an abrupt change in the stimulus. Although APD and its rate dependence in tissue might be modulated by the effect of stimulation rate on extracellular K^+ concentration dynamics, previous studies suggest that these effects are not expected to play a major role in mammalian ventricular muscle (7).

Furthermore, in the present article, we aimed to analyze the effect of the main transmembrane currents of the TP06 ionic model involved in AP repolarization on the main cellular biomarkers of arrhythmic risk. We have focused on analyzing the role of the maximum conductance and kinetics of the main transmembrane ionic currents involved in repolarization in modulating electrophysiological properties associated with arrhythmic risk. Additional model parameters, such as steady-state values of the gates, may also influence the cellular electrophysiological characteristics. The influence of the fast Na^+ current has not been commented in the manuscript because, as expected (7), its effect on the biomarkers studied in this study was negligible. This was confirmed by our simulations (results not shown). Indeed, it is well known that the primary role of the fast Na^+ current is in the depolarization phase of the AP. However, as drug-induced effects on Na^+ channels might exert a critical influence in arrhythmias (9, 10, 20, 35), further research on the influence of the fast Na^+ current properties in properties such as AP depolarization, the conduction velocity or safety factor of propagation (45, 49) would be very valuable. In addition, although the late Na^+ current might be important in TdP generation, its role has not been studied in this article since it is not included in the TP06 model. Furthermore, a complete study of drug-receptor interactions for each current and their rate-dependent effects was beyond the scope of the present study. Finally, interesting conclusions would arise from the study of the ion basis of the main preclinical biomarkers of arrhythmic risk under pathological conditions such as ischemia or heart failure, when cardiac arrhythmias are likely to appear.

Conclusions

This study provides new insights into the ionic basis of the electrophysiological biomarkers used to assess arrhythmic risk preclinically. More specifically, the simulation results provide a systematic investigation into how changes in specific ionic current properties (which could be caused by natural variability, genetic mutations, or drug-induced alterations) can modu-

late APD, AP triangulation, restitution properties, APD rate adaptation as well as $[Ca^{2+}]_i$ and $[Na^+]_i$, and its rate dependence. A comparison of the simulation results to the experimental data demonstrates that the sensitivity analysis performed here is a powerful method for the systematic and in-depth validation of AP models. It also highlights the need for additional experimental data to further our understanding of human ventricular myocyte electrophysiology.

ACKNOWLEDGMENTS

We thank Dr. Kirsten ten Tusscher and Profs. David Gavaghan and Kevin Burrage for useful discussions. We are also grateful to the Oxford e-Research Center for the use made of their Microsoft cluster to run the simulations.

GRANTS

This study was supported financially by the European Commission preDiCT Grant DG-INFOS-224381, a UK Medical Research Council Career Development award (to B. Rodríguez), Royal Society Visiting Fellowships (to L. Romero and E. Pueyo), a Conselleria de Educació grant (Generalitat Valenciana to L. Romero), Ministerio de Ciencia e Innovación Grants TEC-2005-04199 and TEC-2008-02090 (to L. Romero) and TEC-2007-68076-C02-02 (to E. Pueyo) (Spain), and from Caja de Ahorros de la Inmaculada (to E. Pueyo).

REFERENCES

1. **Bavendiek U, Brixius K, Munch G, Zobel C, Muller-Ehmsen J, Schwinger RH.** Effect of inotropic interventions on the force-frequency relation in the human heart. *Basic Res Cardiol* 93, Suppl 1: 76–85, 1998.
2. **Bers DM, Despa S.** Cardiac myocytes Ca^{2+} and Na^+ regulation in normal and failing hearts. *J Pharm Sci* 100: 315–322, 2006.
3. **Beuckelmann DJ, Nabauer M, Erdmann E.** Intracellular calcium handling in isolated ventricular myocytes from patients with terminal heart failure. *Circulation* 85: 1046–1055, 1992.
4. **Biliczki P, Virag L, Iost N, Papp JG, Varro A.** Interaction of different potassium channels in cardiac repolarization in dog ventricular preparations: role of repolarization reserve. *Br J Pharmacol* 137: 361–368, 2002.
5. **Bosch RF, Gaspo R, Busch AE, Lang HJ, Li GR, Nattel S.** Effects of the chromanol 293B, a selective blocker of the slow, component of the delayed rectifier K^+ current, on repolarization in human and guinea pig ventricular myocytes. *Cardiovasc Res* 38: 441–450, 1998.
6. **Boyett MR, Fedida D.** Changes in the electrical activity of dog cardiac Purkinje fibres at high heart rates. *J Physiol* 350: 361–391, 1984.
7. **Boyett MR, Jewell BR.** Analysis of the effects of changes in rate and rhythm upon electrical activity in the heart. *Prog Biophys Mol Biol* 36: 1–52, 1980.
8. **Brixius K, Pietsch M, Hoischen S, Muller-Ehmsen J, Schwinger RH.** Effect of inotropic interventions on contraction and Ca^{2+} transients in the human heart. *J Appl Physiol* 83: 652–660, 1997.
9. **Clancy CE, Wehrens XH.** Mutation-specific effects of lidocaine in Brugada syndrome. *Int J Cardiol* 121: 249–252, 2007.
10. **Clancy CE, Zhu ZI, Rudy Y.** Pharmacogenetics and anti-arrhythmic drug therapy: a theoretical investigation. *Am J Physiol Heart Circ Physiol* 292: H66–H75, 2007.
11. **Dangman KH, Danilo P Jr, Hordof AJ, Mary-Rabine L, Reder RF, Rosen MR.** Electrophysiologic characteristics of human ventricular and Purkinje fibers. *Circulation* 65: 362–368, 1982.
12. **Drouin E, Charpentier F, Gauthier C, Laurent K, Le Marec H.** Electrophysiologic characteristics of cells spanning the left ventricular wall of human heart: evidence for presence of M cells. *J Am Coll Cardiol* 26: 185–192, 1995.
13. **Faber GM, Rudy Y.** Action potential and contractility changes in $[Na^+]_i$ overloaded cardiac myocytes: a simulation study. *Biophys J* 78: 2392–2404, 2000.
14. **Fink M, Noble D, Virag L, Varro A, Giles WR.** Contributions of HERG K^+ current to repolarization of the human ventricular action potential. *Prog Biophys Mol Biol* 96: 357–376, 2008.
15. **Fox JJ, McHarg JL, Gilmour RF Jr.** Ionic mechanism of electrical alternans. *Am J Physiol Heart Circ Physiol* 282: H516–H530, 2002.
16. **Franz MR, Swerdlow CD, Liem LB, Schaefer J.** Cycle length dependence of human action potential duration in vivo. Effects of single extrastimuli, sudden sustained rate acceleration and deceleration, and different steady-state frequencies. *J Clin Invest* 82: 972–979, 1988.

18. Fulop L, Banyasz T, Magyar J, Szentandrassy N, Varro A, Nanasi PP. Reopening of L-type calcium channels in human ventricular myocytes during applied epicardial action potentials. *Acta Physiol Scand* 180: 39–47, 2004.
19. Garfinkel A, Kim YH, Voroshilovsky O, Qu Z, Kil JR, Lee MH, Karagueuzian HS, Weiss JN, Chen PS. Preventing ventricular fibrillation by flattening cardiac restitution. *Proc Natl Acad Sci USA* 97: 6061–6066, 2000.
20. Glaaser IW, Clancy CE. Cardiac Na⁺ channels as therapeutic targets for antiarrhythmic agents. *Handb Exp Pharmacol* 99–121, 2006.
21. Guo D, Zhou J, Zhao X, Gupta P, Kowey PR, Martin J, Wu Y, Liu T, Yan GX. L-type calcium current recovery versus ventricular repolarization: preserved membrane-stabilizing mechanism for different QT intervals across species. *Heart Rhythm* 5: 271–279, 2008.
22. Hasenfuss G, Schillinger W, Lehnart SE, Preuss M, Pieske B, Maier LS, Prestle J, Minami K, Just H. Relationship between Na⁺-Ca²⁺-exchanger protein levels and diastolic function of failing human myocardium. *Circulation* 99: 641–648, 1999.
23. Holubarsch C, Ludemann J, Wiessner S, Ruf T, Schulte-Baukloh H, Schmidt-Schweda S, Pieske B, Posival H, Just H. Shortening versus isometric contractions in isolated human failing and non-failing left ventricular myocardium: dependency of external work and force on muscle length, heart rate and inotropic stimulation. *Cardiovasc Res* 37: 46–57, 1998.
24. Hondeghem LM, Carlsson L, Duker G. Instability and triangulation of the action potential predict serious proarrhythmia, but action potential duration prolongation is antiarrhythmic. *Circulation* 103: 2004–2013, 2001.
25. Hua F, Gilmour RF Jr. Contribution of I_{Kr} to rate-dependent action potential dynamics in canine endocardium. *Circ Res* 94: 810–819, 2004.
26. Hua F, Johns DC, Gilmour RF Jr. Suppression of electrical alternans by overexpression of HERG in canine ventricular myocytes. *Am J Physiol Heart Circ Physiol* 286: H2342–H2351, 2004.
27. Hund TJ, Kucera JP, Otani NF, Rudy Y. Ionic charge conservation and long-term steady state in the Luo-Rudy dynamic cell model. *Biophys J* 81: 3324–3331, 2001.
28. Iost N, Virag L, Opincariu M, Szecsi J, Varro A, Papp JG. Delayed rectifier potassium current in undiseased human ventricular myocytes. *Cardiovasc Res* 40: 508–515, 1998.
29. Jost N, Virag L, Bitay M, Takacs J, Lengyel C, Biliczki P, Nagy Z, Bogats G, Lathrop DA, Papp JG, Varro A. Restricting excessive cardiac action potential and QT prolongation: a vital role for I_{Ks} in human ventricular muscle. *Circulation* 112: 1392–1399, 2005.
30. Lau CP, Freedman AR, Fleming S, Malik M, Camm AJ, Ward DE. Hysteresis of the ventricular paced QT interval in response to abrupt changes in pacing rate. *Cardiovasc Res* 22: 67–72, 1988.
31. Lawrence CL, Pollard CE, Hammond TG, Valentin JP. Nonclinical proarrhythmia models: predicting Torsades de Pointes. *J Pharmacol Toxicol Methods* 52: 46–59, 2005.
32. Levi AJ, Dalton GR, Hancox JC, Mitcheson JS, Issberner J, Bates JA, Evans SJ, Howarth FC, Hobai IA, Jones JV. Role of intracellular sodium overload in the genesis of cardiac arrhythmias. *J Cardiovasc Electrophysiol* 8: 700–721, 1997.
33. Li GR, Feng J, Yue L, Carrier M. Transmural heterogeneity of action potentials and I_{to1} in myocytes isolated from the human right ventricle. *Am J Physiol Heart Circ Physiol* 275: H369–H377, 1998.
34. Li GR, Yang B, Feng J, Bosch RF, Carrier M, Nattel S. Transmembrane I_{Ca} contributes to rate-dependent changes of action potentials in human ventricular myocytes. *Am J Physiol Heart Circ Physiol* 276: H98–H106, 1999.
35. Liu H, Tateyama M, Clancy CE, Abriel H, Kass RS. Channel openings are necessary but not sufficient for use-dependent block of cardiac Na⁺ channels by flecainide: evidence from the analysis of disease-linked mutations. *J Gen Physiol* 120: 39–51, 2002.
36. Murphy E, Eisner DA. Regulation of intracellular and mitochondrial sodium in health and disease. *Circ Res* 104: 292–303, 2009.
37. Narayan SM, Bayer JD, Lalani G, Trayanova NA. Action potential dynamics explain arrhythmic vulnerability in human heart failure: a clinical and modeling study implicating abnormal calcium handling. *J Am Coll Cardiol* 52: 1782–1792, 2008.
38. Nash MP, Bradley CP, Sutton PM, Clayton RH, Kallis P, Hayward MP, Paterson DJ, Taggart P. Whole heart action potential duration restitution properties in cardiac patients: a combined clinical and modeling study. *Exp Physiol* 91: 339–354, 2006.
39. Nolasco JB, Dahlen RW. A graphic method for the study of alternation in cardiac action potentials. *J Appl Physiol* 25: 191–196, 1968.
40. Pieske B, Maier LS, Bers DM, Hasenfuss G. Ca²⁺ handling and sarcoplasmic reticulum Ca²⁺ content in isolated failing and nonfailing human myocardium. *Circ Res* 85: 38–46, 1999.
41. Pieske B, Maier LS, Piacentino V 3rd, Weisser J, Hasenfuss G, Houser S. Rate dependence of [Na⁺]_i and contractility in nonfailing and failing human myocardium. *Circulation* 106: 447–453, 2002.
- 41a. Pueyo E, Laguna P, Rodríguez B. Mechanisms of ventricular heart rate adaptation as an indicator of arrhythmic risk (Conference Proceeding). *Heart Rhythm* 5, suppl 1, S162, 2008.
42. Pueyo E, Smetana P, Caminal P, de Luna AB, Malik M, Laguna P. Characterization of QT interval adaptation to RR interval changes and its use as a risk-stratifier of arrhythmic mortality in amiodarone-treated survivors of acute myocardial infarction. *IEEE Trans Biomed Eng* 51: 1511–1520, 2004.
43. Riccio ML, Koller ML, Gilmour RF Jr. Electrical restitution and spatiotemporal organization during ventricular fibrillation. *Circ Res* 84: 955–963, 1999.
44. Roden DM. Repolarization reserve: a moving target. *Circulation* 118: 981–982, 2008.
45. Romero L, Trénor B, Alonso JM, Tobón C, Saiz J, Ferrero JM Jr. The relative role of refractoriness and source-sink relationship in reentry generation during simulated acute ischemia. *Ann Biomed Eng* 37: 1560–1571, 2009.
46. Schmidt U, Hajjar RJ, Helm PA, Kim CS, Doye AA, Gwathmey JK. Contribution of abnormal sarcoplasmic reticulum ATPase activity to systolic and diastolic dysfunction in human heart failure. *J Mol Cell Cardiol* 30: 1929–1937, 1998.
47. Schmitt C, Brachmann J, Karch M, Waldecker B, Navarrete L, Montero M, Beyer T, Kubler W. Reverse use-dependent effects of sotalol demonstrated by recording monophasic action potentials of the right ventricle. *Am J Cardiol* 68: 1183–1187, 1991.
48. Schwinger RH, Muller-Ehmsen J, Frank K, Koch A, Erdmann E. Enhanced sensitivity of the failing human myocardium to cardiac glycosides and Na⁺-channel activators. *Am Heart J* 131: 988–993, 1996.
49. Shaw RM, Rudy Y. Ionic mechanisms of propagation in cardiac tissue. Roles of the sodium and L-type calcium currents during reduced excitability and decreased gap junction coupling. *Circ Res* 81: 727–741, 1997.
50. Sims C, Reisenweber S, Viswanathan PC, Choi BR, Walker WH, Salama G. Sex, age, and regional differences in L-type calcium current are important determinants of arrhythmia phenotype in rabbit hearts with drug-induced long QT type 2. *Circ Res* 102: e86–e100, 2008.
51. Stengl M, Ramakers C, Donker DW, Nabar A, Rybin AV, Spätjens RL, van der Nagel T, Wodzig WK, Sipido KR, Antoons G, Moorman AF, Vos MA, Volders PG. Temporal patterns of electrical remodeling in canine ventricular hypertrophy: focus on I_{Ks} downregulation and blunted beta-adrenergic activation. *Cardiovasc Res* 72: 90–100, 2006.
52. Szentandrassy N, Banyasz T, Biro T, Szabo G, Toth BI, Magyar J, Lazar J, Varro A, Kovacs L, Nanasi PP. Apico-basal inhomogeneity in distribution of ion channels in canine and human ventricular myocardium. *Cardiovasc Res* 65: 851–860, 2005.
53. ten Tusscher KH, Hren R, Panfilov AV. Organization of ventricular fibrillation in the human heart. *Circ Res* 100: e87–e101, 2007.
54. ten Tusscher KH, Noble D, Noble PJ, Panfilov AV. A model for human ventricular tissue. *Am J Physiol Heart Circ Physiol* 286: H1573–H1589, 2004.
55. ten Tusscher KH and Panfilov AV. Alternans and spiral breakup in a human ventricular tissue model. *Am J Physiol Heart Circ Physiol* 291: H1088–H1100, 2006.
56. Tolkacheva EG, Anumonwo JM, Jalife J. Action potential duration restitution portraits of mammalian ventricular myocytes: role of calcium current. *Biophys J* 91: 2735–2745, 2006.
57. Verkerk AO, Wilders R, Veldkamp MW, de Geringel W, Kirkels JH, Tan HL. Gender disparities in cardiac cellular electrophysiology and arrhythmia susceptibility in human failing ventricular myocytes. *Int Heart J* 46: 1105–1118, 2005.
58. Virag L, Iost N, Opincariu M, Szolnoky J, Szecsi J, Bogats G, Szenohradzky P, Varro A, Papp JG. The slow component of the delayed rectifier potassium current in undiseased human ventricular myocytes. *Cardiovasc Res* 49: 790–797, 2001.
59. Volders PG, Vos MA, Szabo B, Sipido KR, de Groot SH, Gorgels AP, Wellens HJ, Lazzara R. Progress in the understanding of cardiac early afterdepolarizations and torsades de pointes: time to revise current concepts. *Cardiovasc Res* 46: 376–392, 2000.
60. Weiss JN, Karma A, Shiferaw Y, Chen PS, Garfinkel A, Qu Z. From pulsus to pulseless: the saga of cardiac alternans. *Circ Res* 98: 1244–1253, 2006.
61. Xiao L, Xiao J, Luo X, Lin H, Wang Z, Nattel S. Feedback remodeling of cardiac potassium current expression: a novel potential mechanism for control of repolarization reserve. *Circulation* 118: 983–992, 2008.